Superconductivity from orbital-selective electron-phonon coupling in AV_3Sb_5

Ethan T. Ritz,[1] Henrik S. Røising [ORCID],[2] Morten H. Christensen,[2] Turan Birol,[1] Brian M. Andersen [ORCID],[2] and Rafael M. Fernandes[3]

[1]*Department of Chemical Engineering and Materials Science, University of Minnesota, Minnesota 55455, USA*
[2]*Niels Bohr Institute, University of Copenhagen, DK-2200 Copenhagen, Denmark*
[3]*School of Physics and Astronomy, University of Minnesota, Minneapolis, Minnesota 55455, USA*

Recent experiments have shown that the phase diagrams of the kagome superconductors AV_3Sb_5 are strongly impacted by changes in the c-axis lattice parameter. Here, we show that c-axis deformations impact primarily the Sb apical bonds and thus the overlap between their p_z orbitals. Changes in the latter, in turn, substantially affect low-energy electronic states with significant Sb character, most notably the central electron pocket and the van Hove singularities located above the Fermi level. Based on the orbital-selective character of c-axis strain, we argue that these electronic states experience a non-negligible attractive electron-phonon pairing interaction mediated by fluctuations in the apical Sb bonds. We thus propose a multiband model for superconductivity in AV_3Sb_5 that includes both the Sb pocket and the V-derived van Hove singularities. Upon comparing the theoretical phase diagram with the experimentally observed vanishing of the T_c dome across a Lifshitz transition of the Sb pocket, we propose that either an s^{+-} or an s^{++} state is realized in AV_3Sb_5.

The discovery of superconductivity (SC) in the family of kagome metals AV_3Sb_5 (A: K, Rb, Cs) has sparked significant interest since the interference between different electronic hopping paths in the kagome lattice endows the electronic structure with flat bands, van Hove singularities (vHs), and Dirac points. These features have the potential to promote collective electronic behavior characteristic of materials with strong electronic correlations or nontrivial band topology [1–4]. Indeed, upon a cursory examination, the phase diagrams of AV_3Sb_5 resemble those of Cu- and Fe-based superconductors, in that SC appears in close proximity to another electronic order, in this case a charge-density wave (CDW) phase, which has been intensely scrutinized both theoretically [5–11] and experimentally [12–16]. While the three-dimensional nature of the CDW wave-vector is well established [17–20], there remains considerable debate whether it also breaks time-reversal and rotational symmetries [21–28].

Studies of the SC properties of AV_3Sb_5 have lagged the investigations of the CDW phase, partly because the latter onsets at much higher temperatures ($T_{CDW} \approx 100$ K) than the former ($T_c \approx 1$ K). There have been reports of both nodeless [29–35] and nodal [15,36,37] gap structures, as well as conflicting accounts of whether the electron-phonon coupling can explain the SC instability [38–41]. Proposals have been put forward in favor of both conventional and unconventional pairing, most of which focus on the electronic states derived from the V d orbitals [5,6,8,42–46], which give rise to saddle points in the band structure near the M point. However, recent experimental studies of the doping-temperature and pressure-temperature phase diagrams of CsV_3Sb_5 have shown that the end of the SC dome in either case coincides with the disappearance of an electron pocket at the Γ point derived from the Sb p orbitals, highlighting their relevance for the onset of pairing [47,48].

In this paper, we combine density-functional theory (DFT) calculations and low-energy modeling to show that the Sb degrees of freedom play an essential role for the superconductivity of AV_3Sb_5. Our starting point is the empirical observation made in Ref. [49] that the phase diagrams of CsV_3Sb_5 under pressure and under uniaxial in-plane stress fall essentially on top of each other when T_{CDW} and T_c are expressed as a function of the c-axis expansion or contraction. Moreover, thermal expansion measurements report a c-axis response much more pronounced than the a-axis response at both T_c and T_{CDW} [50]. These results are strong indication that the c-axis lattice parameter is a key control parameter for both types of electronic order. From DFT, we find that the states primarily affected by changes in the c axis are those that have a significant contribution from the apical Sb orbitals: the vHs above the Fermi level at the M point and the electron band centered at the Γ point, whose bottom shifts by hundreds of meV for strain values of a few percent. In contrast, the energies of the vHs below the Fermi level remain nearly unchanged. Such an "orbital-selective" modification of the electronic spectrum provides a mechanism by which the c-axis lattice parameter can impact the CDW and SC transitions, as empirically seen in Ref. [49]. Based on these results, we construct a low-energy model for the SC state of AV_3Sb_5 consisting of a central Sb-dominated electron pocket and a large V-dominated Fermi surface associated with the vHs. By studying the evolution of T_c as the Sb band raises above the Fermi level, we find that only s^{++} and s^{+-} states are compatible with the observation of a vanishing T_c as the Sb pocket undergoes a Lifshitz transition, in agreement with experiments [47,48].

We start by employing DFT to elucidate the impact of c-axis distortions on the band structure of AV_3Sb_5, focusing on $A = Cs$ for concreteness. For details, see the Supplemental Material (SM) [51]. Above T_{CDW} and at ambient pressure, CsV_3Sb_5 adopts the $P6/mmm$ (#191) space group, with Cs
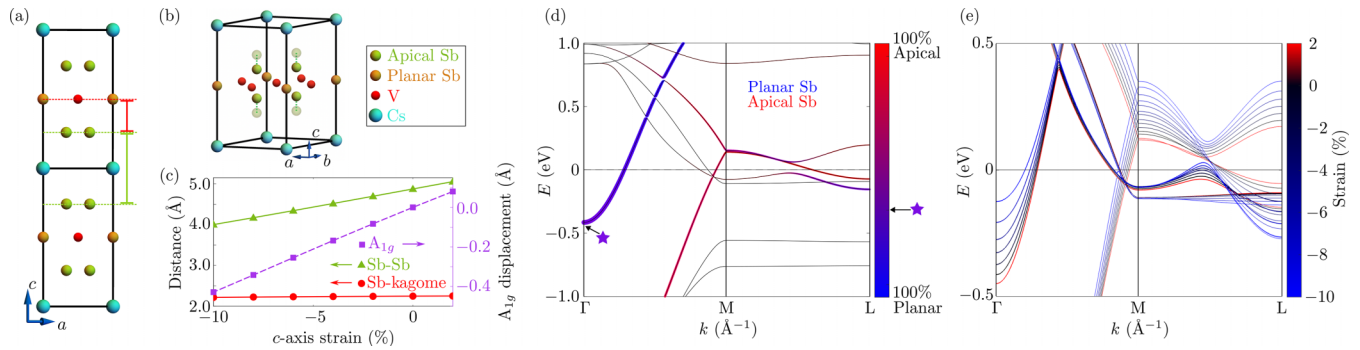
FIG. 1. [(a), (b)] Schematic illustrations of two neighboring AV_3Sb_5 unit cells and of the displacement pattern of the apical Sb promoted by the A_{1g} phonon mode, respectively. We choose a sign convention such that the displacement of apical Sb towards the kagome plane corresponds to positive A_{1g}. (c) Changes in the distances between the Sb apical atom and its nearest-neighbor (green triangles) and the V atoms (red circles) as a function of c-axis strain for CsV_3Sb_5. The purple squares give the atomic displacements from the equilibrium structure corresponding to a frozen excitation of the optical A_{1g} phonon mode. (d) Low-energy band structure of CsV_3Sb_5. The thickness of the bands is proportional to the total projection onto the p_z orbitals of the Sb atoms, whereas their color is proportional to the projection onto the planar Sb (blue) and apical Sb (red). The Γ band has contributions from both Sb sites. (e) Modifications in the low-energy band structure as a function of c-axis strain. The momentum L is located above M in the hexagonal Brillouin zone; the other momenta are defined in Fig. 2(a).

occupying the $1a$ Wyckoff site, V the $3g$ site, and Sb the $4h$ (apical) and $1b$ (planar) sites, as illustrated in Figs. 1(a) and 1(b). The V atoms form a kagome sublattice, whereas the planar (apical) Sb atoms, a hexagonal (honeycomb) sublattice. Besides the lattice parameters, the reduced z coordinate of the apical Sb atoms is the only free structural parameter. Interestingly, z increases significantly upon compression of the c axis in a way that approximately preserves the Sb–V bond distances between the apical Sb and the kagome layer, while shortening the Sb–Sb bond distances between apical Sb in adjacent unit cells, as shown Fig. 1(c).

To address whether this displacement pattern is capable of affecting the low-energy electronic states, we first calculate via DFT the atomically resolved band structure near the Fermi energy in the undistorted phase [Fig. 1(d)]. In agreement with previous works [47,48,59], we find dominant spectral-weight contributions from both types of Sb atoms (planar and apical) to the Γ-point electron band, as well as a significant contribution from the apical Sb to the V-dominated saddle points located above the Fermi level at the M point. It is this hybridization between apical Sb orbitals and V orbitals that endow the corresponding vHs with a significant k_z dispersion, to the point that they even cross the Fermi level along the M-L line.

In Fig. 1(e), we show how the low-energy band structure is modified by both compressive (negative) and tensile (positive) c-axis strain (see also Ref. [60]). We include large absolute values of strain to highlight the effect. Note that all internal lattice parameters are relaxed for a given c-axis distortion, while keeping the in-plane lattice parameter fixed. The bands that are most affected are those exhibiting a sizable contribution from the apical Sb atoms, such as the vHs located above the Fermi level. Since the CDW is associated with the condensation of phonon modes at the M and L points [9,17], this provides a possible mechanism by which c-axis strain can impact the CDW phase. Besides these saddle points, the bottom of the electron pocket at the Γ point moves substantially with c-axis changes, with shifts of 100 meV for strains of about 1% (see also Fig. S1 in the SM [51]). In contrast, the

energies of the M-point vHs located below the Fermi level barely change, reflecting their dominant V character. The large shifts of the bottom of the Γ-point electron band can be attributed to the out-of-phase overlap between the p_z orbitals of apical Sb atoms of neighboring unit cells. This overlap generates a bonding and an antibonding state, the latter of which gives rise to the Γ-point electron band. Upon compression of the c axis, the orbital overlap increases and, consequently, the energy of the antibonding state increases, leading to the observed shift in the bottom of the electron band.

The electronic properties of AV_3Sb_5 should be impacted not only by static strain, but also by thermal fluctuations associated with the atomic displacement pattern promoted by the c-axis strain. These fluctuations are expected to be strongly coupled to the electronic states with significant Sb character. Because the displacement pattern associated with the Sb–Sb bonds does not break crystal symmetries, it cannot be decomposed in terms of a single phonon mode. Instead, there are two different phonon modes that modify the bond lengths along the c axis without modifying other features in the crystal structure: a longitudinal acoustic-phonon mode with out-of-plane dispersion and a Γ-point optical phonon mode that transforms as the A_{1g} irreducible representation of the point group. Note that the A_{1g} displacements, represented in Fig. 1(b), also involve changes in the Sb–V bond distances. As shown in Fig. 1(c), the strong c-axis strain dependence of the displacement associated with this A_{1g} mode resembles that displayed by the Sb–Sb bond distance. This result confirms that the A_{1g} phonon mode leads to Sb–Sb bond fluctuations.

The coupling between the electronic states with significant Sb spectral weight and these phonon modes should lead to a non-negligible attractive pairing interaction. To assess its impact, we construct a low-energy model for the SC phase considering a simplified Fermi surface that consists of a small Sb electron-pocket at the Γ point and a large hexagonal-like Fermi surface originating from one of the V vHs [42,46,47,59]. The V band is modeled in terms of a single orbital on the sites of the kagome lattice whereas the Sb band is parametrized as a nearly isotropic dispersion,
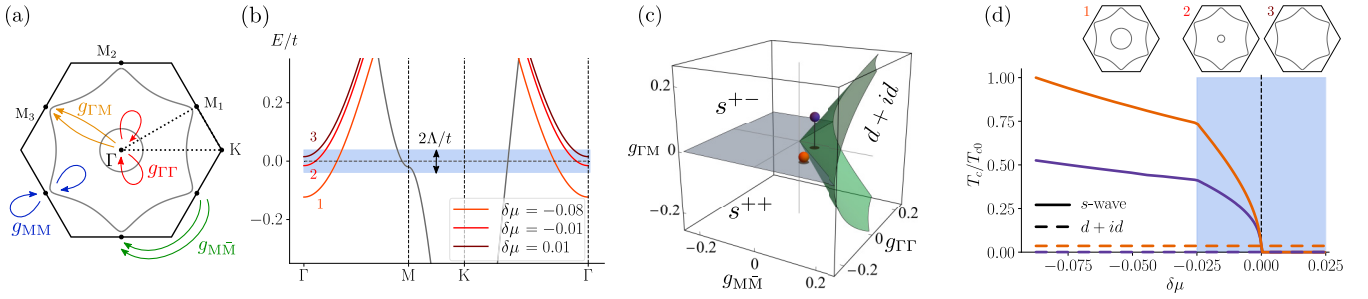
FIG. 2. (a) Pairing interactions of the four-patch model involving fermions at the M_i and Γ points. The Fermi surface is shown in gray. (b) Tight-binding dispersions, highlighting the Lifshitz transition of the Γ-point electron pocket as a function of the parameter $\delta\mu \equiv (\mu_\Gamma - \mu_c)/\mu_c$; Λ is the pairing interaction cutoff. (c) SC phase diagram of the four-patch model (away from the Lifshitz transition) as a function of the interactions shown in panel (a); s-wave corresponds to either s^{++} or s^{+-} states depending on the sign of $g_{\Gamma M}$. (d) T_c as a function of the parameter $\delta\mu$ that tunes the Γ pocket across the Lifshitz transition at $\delta\mu = 0$, as shown in the insets. The interaction parameters, marked by the orange and purple symbols shown in panel (c), are $(g_{M\bar{M}}, g_{\Gamma M}, g_{\Gamma\Gamma}, g_{MM}) = (0.1, 0.015, -0.15, 0)$ for the orange lines and $(0.07, 0.1, -0.03, 0)$ for the purple lines. T_{c0} is the SC transition temperature for the first set of parameters (orange) at $\mu_{\Gamma 0} = -3.65\tilde{t}$.

$\xi_\Gamma(\boldsymbol{k}) = \tilde{t} f_\Gamma(\boldsymbol{k}) - \mu_\Gamma$; details are given in the SM [51]. The parameter μ_Γ defines the energy of the bottom of the electron band and is set to $\mu_{\Gamma 0} = -3.65\tilde{t}$ for the undistorted compound based on comparison with angle-resolved photoemission spectroscopy (ARPES) measurements [61]. Upon decreasing μ_Γ, which mimics the effect of hole doping, a Lifshitz transition occurs at $\mu_c \equiv -4\tilde{t}$, where the Γ-point Fermi pocket disappears. For simplicity, we thus define $\delta\mu \equiv (\mu_\Gamma - \mu_c)/\mu_c$.

To derive the SC gap equations, we generalize a patch approach commonly employed to describe systems with vHs near the Fermi level [62–67]. Because of the logarithmic enhancement of the density of states (DOS) at the M-point vHs, it is sufficient to consider only the pairing interactions involving states on the three Fermi-surface patches centered at each of the three M points. Symmetry restricts these interactions to two different types: intrapatch g_{MM}/N_M and interpatch $g_{M\bar{M}}/N_M$, where N_M is the DOS of the M-point patches. We approximate the small Γ pocket by a fourth patch subjected to an intrapatch pairing interaction $g_{\Gamma\Gamma}/N_\Gamma$ and an interpatch interaction $g_{\Gamma M}/\sqrt{N_M N_\Gamma}$ with the M-point patches. Based on our results above, we assume an attractive interaction $g_{\Gamma\Gamma} < 0$ arising from the electron-phonon coupling involving the apical Sb degrees of freedom. Note that this parametrization of the pairing interaction in terms of the DOS of each patch is not valid close to the Lifshitz transition; we will return to this point later.

The resulting four-patch model is schematically shown in Fig. 2(a). Denoting $\vec{\Delta} \equiv (\Delta_{M_1}, \Delta_{M_2}, \Delta_{M_3}, \Delta_\Gamma)^T$ for the gap functions on the four patches, the corresponding linearized gap equations can be written in matrix form as $\chi_{pp}\vec{\Delta} = \vec{\Delta}$, with

$$\chi_{pp} = -V_\Lambda \begin{bmatrix} g_{MM} & g_{M\bar{M}} & g_{M\bar{M}} & \eta g_{\Gamma M} \\ g_{M\bar{M}} & g_{MM} & g_{M\bar{M}} & \eta g_{\Gamma M} \\ g_{M\bar{M}} & g_{M\bar{M}} & g_{MM} & \eta g_{\Gamma M} \\ \eta^{-1}g_{\Gamma M} & \eta^{-1}g_{\Gamma M} & \eta^{-1}g_{\Gamma M} & g_{\Gamma\Gamma} \end{bmatrix}, \quad (1)$$

where $V_\Lambda \equiv \int_{-\Lambda}^{\Lambda} d\varepsilon \tanh(\beta\varepsilon/2)/(2\varepsilon) \approx \ln(2e^\gamma \beta\Lambda/\pi)$ is the particle-particle bubble with $\beta = 1/(k_B T)$ and $\eta \equiv \sqrt{N_\Gamma/N_M}$ is the ratio between the DOS. Here, Λ is the cutoff for the pairing interaction, as shown in Fig. 2(b), and $\gamma \approx 0.577$ is

Euler's constant. T_c is found by imposing that the largest eigenvalue of χ_{pp} is 1. The two leading eigenvalues are

$$\lambda_{E_{2g}} = (g_{M\bar{M}} - g_{MM}) \ln(2e^\gamma \beta\Lambda/\pi), \quad (2)$$

$$\lambda_{A_{1g}} = \tfrac{1}{2}(\tilde{g} - 2g_{M\bar{M}} - g_{MM} - g_{\Gamma\Gamma}) \ln(2e^\gamma \beta\Lambda/\pi), \quad (3)$$

where $\tilde{g} \equiv \sqrt{12g_{\Gamma M}^2 + (g_{\Gamma\Gamma} - 2g_{M\bar{M}} - g_{MM})^2}$. Analysis of the eigenvectors of $\lambda_{E_{2g}}$, which is doubly degenerate, shows that they describe $d_{x^2-y^2}$-wave and d_{xy}-wave SC states, which transform as the two-dimensional (2D) irreducible representation E_{2g} of the point group D_{6h} (see SM [51]). As discussed elsewhere [62], going beyond the linearized gap equation reveals that the linear combination $d_{x^2-y^2} \pm id_{xy}$ minimizes the free energy, leading to a time-reversal symmetry-breaking SC phase. The second eigenvalue $\lambda_{A_{1g}}$ corresponds to a pairing state that transforms as the trivial representation A_{1g}, corresponding to two isotropic gaps Δ_Γ and Δ_M. While the symmetry of this state is s wave, there are two qualitatively different possible gap configurations depending on the signs of Δ_Γ and Δ_M: an s^{++} state, in the case of equal signs, or an s^{+-} state, in the case of opposite signs—similar to that realized in the Fe-based superconductors [68].

Only positive eigenvalues correspond to attractive pairing channels. For the E_{2g} channel ($d + id$), $\lambda_{E_{2g}} > 0$ requires a strong enough inter-M-patch repulsion to overcome the intra-M-patch repulsion, $g_{M\bar{M}} > g_{MM} > 0$, as found in renormalization-group studies of the three-patch model [62]. As for the A_{1g} channel (s^{++} or s^{+-}), $\lambda_{A_{1g}} > 0$ requires either a strong interpatch interaction $g_{\Gamma M}$, which can be repulsive or attractive, or a strong intra-Γ-patch attraction $g_{\Gamma\Gamma} < 0$. Note that the sign of $g_{\Gamma M}$ does not impact the eigenvalue $\lambda_{A_{1g}}$, but only whether the eigenvector corresponds to the s^{++} ($g_{\Gamma M} < 0$) or the s^{+-} ($g_{\Gamma M} > 0$) state (see SM [51]).

Figure 2(c) shows the SC phase diagram in the $\{g_{M\bar{M}}, g_{\Gamma\Gamma}, g_{\Gamma M}\}$ parameter space. As anticipated, the $d + id$ state is only stabilized by a dominant repulsive interaction $g_{M\bar{M}} > 0$, whereas attractive interactions of any kind favor an s-wave state. An increase in the magnitude of the interpatch interaction $g_{\Gamma M}$, be it attractive or repulsive, further expands the regime where the s-wave state is realized. While this plot is obtained for $g_{MM} = 0$, the main effect of a nonzero g_{MM} is

in the case where it is repulsive, as it suppresses the regime in which SC is stabilized (see SM [51]).

To elucidate which of these SC regimes are consistent with the experimental observation of a suppression of T_c across the Lifshitz transition [47,48], we compute the evolution of T_c as μ_Γ approaches the critical value μ_c for which the electron-band bottom crosses the Fermi level (see inset of Fig. 2(d)). Near the Lifshitz transition, where $|\mu_\Gamma - \mu_c| \ll \Lambda$, the gap equations (1) have to be modified, as it is not justified to remove the DOS from the integrand of the particle-particle bubble [69,70]. The modified χ_{pp} is shown in the SM [51]. By numerically computing its eigenvalues, we obtain $T_c(\mu_\Gamma)$ for the various regimes in Fig. 2(c). Because the $d + id$ state is insensitive to the Γ pocket, its T_c does not change across the Lifshitz transition. Meanwhile, the behavior of T_c of the s-wave state depends on the nature of the dominant pairing interaction. If the s-wave state is driven by large attractive interactions involving the M patches only, $g_{M\bar{M}}$, $g_{MM} < 0$, T_c is not significantly changed at μ_c. On the other hand, for dominant intra-Γ-patch attraction $g_{\Gamma\Gamma} < 0$ or dominant inter-patch $g_{\Gamma M}$ of either sign, T_c is strongly suppressed across the Lifshitz transition. This is shown in Fig. 2(d) for the parameter values corresponding to the orange symbol (dominant $g_{\Gamma\Gamma}$) and the purple symbol (dominant $g_{\Gamma M}$) in Fig. 2(c). Additional $T_c(\mu_\Gamma)$ plots for other parameter values are shown in the SM [51].

A large attractive intrapocket pairing interaction $g_{\Gamma\Gamma}$ could be mediated by the Sb–Sb bond fluctuations discussed above. On the other hand, CDW fluctuations with wave vector M could boost $g_{\Gamma M}$, rendering it repulsive (attractive) if the CDW breaks (preserves) time-reversal symmetry. However, these CDW fluctuations should also enhance $g_{M\bar{M}}$, since the M patches are connected by the same wave vector. Because the latter couples states with similar orbital compositions (V-V orbitals), whereas $g_{\Gamma M}$ couples states with different orbital compositions (Sb-V orbitals), the CDW boost of $g_{M\bar{M}}$ is expected to be larger, particularly if the CDW is enhanced by the vHs. Interestingly, the Sb–Sb bond fluctuations could switch this hierarchy if the relevant vHs is one of those located above the Fermi level. Indeed, as shown in Figs. 1(d) and 1(e), those vHs have a sizable Sb orbital weight and as such should be impacted by the phonon modes associated with Sb–Sb bond displacements.

We now discuss the experimental implications of our results. All three states obtained in our model, $d + id$, s^{+-}, and s^{++}, are fully gapped, which makes it challenging to distinguish between them solely via spectroscopy. Directly probing time-reversal symmetry breaking, for instance via Kerr rotation, would help exclude or confirm $d + id$. The suppression of T_c across the Sb electron-pocket Lifshitz transition shown in Fig. 2(d) is qualitatively consistent with the experimental results of Refs. [47,48], suggesting that either an s^{+-} or an s^{++} state is realized, at least in the region of the phase diagram where the CDW is absent. These s-wave states are also compatible with the robustness of T_c against impurities reported in Ref. [32] for CsV_3Sb_5 and with the observed multigap structure of the SC state seen in the parent compounds, where SC coexists with CDW. If one of these gaps is small, it may reconcile reports favoring both a nodeless and a nodal pairing state [29–34,37]. Alternatively, coexistence of an A_{1g} SC state with CDW may lead to nodes in the reconstructed Fermi surface [71]. As for unconventional SC, even if the $d + id$ state is subleading with respect to the s^{+-} or s^{++} channels, interesting mixed states can emerge when the ground states are close in energy. These include not only an $s + d + d$ state that has twofold anisotropy, but also an $s + e^{i\theta}(d + id)$ state that breaks time-reversal symmetry, as discussed in Refs. [65,72]. Due to the presence of inversion symmetry, mixed singlet-triplet states are not expected.

In summary, we showed that changes in the c-axis lattice parameter of AV_3Sb_5 lead to significant changes in the electronic dispersion promoted by the apical Sb p_z orbitals. Not only the energies and the k_z dispersion of the vHs located above the Fermi energy are modified, but also the bottom of the Γ-point electron band shifts strongly with c-axis strain. We proposed that fluctuations of the Sb–Sb bonds promote a non-negligible electron-phonon pairing interaction for states with sizable Sb orbital character, which includes both the central electron pocket as well as the saddle points located above the Fermi level. The resulting s^{+-} and s^{++} states are consistent with several experimental observations, including the full suppression of T_c across the Lifshitz transition involving the Sb pocket [47,48], the nodeless gaps recently observed in ARPES [73], as well as the robustness of T_c against disorder [32,35].

---

[1] J.-X. Yin, S. S. Zhang, H. Li, K. Jiang, G. Chang, B. Zhang, B. Lian, C. Xiang, I. Belopolski, H. Zheng, T. A. Cochran, S.-Y. Xu, G. Bian, K. Liu, T.-R. Chang, H. Lin, Z.-Y. Lu, Z. Wang, S. Jia, W. Wang *et al.*, Giant and anisotropic many-body spin–orbit tunability in a strongly correlated kagome magnet, Nature (London) **562**, 91 (2018).

[2] N. J. Ghimire and I. I. Mazin, Topology and correlations on the kagome lattice, Nat. Mater. **19**, 137 (2020).

[3] M. Kang, L. Ye, S. Fang, J.-S. You, A. Levitan, M. Han, J. I. Facio, C. Jozwiak, A. Bostwick, E. Rotenberg, M. K. Chan, R. D. McDonald, D. Graf, K. Kaznatcheev, E. Vescovo, D. C. Bell, E. Kaxiras, J. van den Brink, M. Richter, M. Prasad Ghimire *et al.*, Dirac fermions and flat bands in the ideal kagome metal FeSn, Nat. Mater. **19**, 163 (2020).

[4] I. F. Gilmutdinov, R. Schönemann, D. Vignolles, C. Proust, I. R. Mukhamedshin, L. Balicas, and H. Alloul, Interplay between

strong correlations and electronic topology in the underlying kagome lattice of $Na_{2/3}CoO_2$, Phys. Rev. B **104**, L201103 (2021).

[5] T. Park, M. Ye, and L. Balents, Electronic instabilities of kagome metals: Saddle points and Landau theory, Phys. Rev. B **104**, 035142 (2021).

[6] Y.-P. Lin and R. M. Nandkishore, Kagome superconductors from Pomeranchuk fluctuations in charge density wave metals, Phys. Rev. B **106**, L060507 (2022).

[7] M. M. Denner, R. Thomale, and T. Neupert, Analysis of Charge Order in the Kagome Metal AV_3Sb_5 (A = K, Rb, Cs), Phys. Rev. Lett. **127**, 217601 (2021).

[8] R. Tazai, Y. Yamakawa, S. Onari, and H. Kontani, Mechanism of exotic density-wave and beyond-Migdal unconventional superconductivity in kagome metal AV_3Sb_5 (A = K, Rb, Cs), Sci. Adv. **8**, eabl4108 (2022).

[9] M. H. Christensen, T. Birol, B. M. Andersen, and R. M. Fernandes, Theory of the charge density wave in AV_3Sb_5 kagome metals, Phys. Rev. B **104**, 214513 (2021).

[10] F. Ferrari, F. Becca, and R. Valentí, Charge density waves in kagome-lattice extended Hubbard models at the van Hove filling, Phys. Rev. B **106**, L081107 (2022).

[11] M. H. Christensen, T. Birol, B. M. Andersen, and R. M. Fernandes, Loop currents in AV_3Sb_5 kagome metals: Multipolar and toroidal magnetic orders, Phys. Rev. B **106**, 144504 (2022).

[12] B. R. Ortiz, L. C. Gomes, J. R. Morey, M. Winiarski, M. Bordelon, J. S. Mangum, I. W. H. Oswald, J. A. Rodriguez-Rivera, J. R. Neilson, S. D. Wilson, E. Ertekin, T. M. McQueen, and E. S. Toberer, New kagome prototype materials: Discovery of KV_3Sb_5, RbV_3Sb_5, and CsV_3Sb_5, Phys. Rev. Mater. **3**, 094407 (2019).

[13] E. M. Kenney, B. R. Ortiz, C. Wang, S. D. Wilson, and M. J. Graf, Absence of local moments in the kagome metal KV_3Sb_5 as determined by muon spin spectroscopy, J. Phys.: Condens. Matter **33**, 235801 (2021).

[14] Y.-X. Jiang, J.-X. Yin, M. M. Denner, N. Shumiya, B. R. Ortiz, G. Xu, Z. Guguchia, J. He, M. S. Hossain, X. Liu, J. Ruff, L. Kautzsch, S. S. Zhang, G. Chang, I. Belopolski, Q. Zhang, T. A. Cochran, D. Multer, M. Litskevich, Z.-J. Cheng *et al.*, Unconventional chiral charge order in kagome superconductor KV_3Sb_5, Nat. Mater. **20**, 1353 (2021).

[15] H. Chen, H. Yang, B. Hu, Z. Zhao, J. Yuan, Y. Xing, G. Qian, Z. Huang, G. Li, Y. Ye, S. Ma, S. Ni, H. Zhang, Q. Yin, C. Gong, Z. Tu, H. Lei, H. Tan, S. Zhou, C. Shen *et al.*, Roton pair density wave in a strong-coupling kagome superconductor, Nature (London) **599**, 222 (2021).

[16] H. Zhao, H. Li, B. R. Ortiz, S. M. L. Teicher, T. Park, M. Ye, Z. Wang, L. Balents, S. D. Wilson, and I. Zeljkovic, Cascade of correlated electron states in the kagome superconductor CsV_3Sb_5, Nature (London) **599**, 216 (2021).

[17] N. Ratcliff, L. Hallett, B. R. Ortiz, S. D. Wilson, and J. W. Harter, Coherent phonon spectroscopy and interlayer modulation of charge density wave order in the kagome metal CsV_3Sb_5, Phys. Rev. Mater. **5**, L111801 (2021).

[18] Q. Stahl, D. Chen, T. Ritschel, C. Shekhar, E. Sadrollahi, M. C. Rahn, O. Ivashko, M. v. Zimmermann, C. Felser, and J. Geck, Temperature-driven reorganization of electronic order in CsV_3Sb_5, Phys. Rev. B **105**, 195136 (2022).

[19] S. Wu, B. R. Ortiz, H. Tan, S. D. Wilson, B. Yan, T. Birol, and G. Blumberg, Charge density wave order in the kagome metal AV_3Sb_5(A = Cs, Rb, K), Phys. Rev. B **105**, 155106 (2022).

[20] M. Kang, S. Fang, J. Yoo, B. R. Ortiz, Y. M. Oey, J. Choi, S. H. Ryu, J. Kim, C. Jozwiak, A. Bostwick, E. Rotenberg, E. Kaxiras, J. G. Checkelsky, S. D. Wilson, J.-H. Park, and R. Comin, Charge order landscape and competition with superconductivity in kagome metals, Nat. Mater. **22**, 186 (2022).

[21] S.-Y. Yang, Y. Wang, B. R. Ortiz, D. Liu, J. Gayles, E. Derunova, R. Gonzalez-Hernandez, L. Šmejkal, Y. Chen, S. S. P. Parkin, S. D. Wilson, E. S. Toberer, T. McQueen, and M. N. Ali, Giant, unconventional anomalous Hall effect in the metallic frustrated magnet candidate, KV_3Sb_5, Sci. Adv. **6**, eabb6003 (2020).

[22] Y. Xiang, Q. Li, Y. Li, W. Xie, H. Yang, Z. Wang, Y. Yao, and H.-H. Wen, Twofold symmetry of c-axis resistivity in topological kagome superconductor CsV_3Sb_5 with in-plane rotating magnetic field, Nat. Commun. **12**, 6727 (2021).

[23] C. Mielke III, D. Das, J.-X. Yin, H. Liu, R. Gupta, Y.-X. Jiang, M. Medarde, X. Wu, H. C. Lei, J. Chang, P. Dai, Q. Si, H. Miao, R. Thomale, T. Neupert, Y. Shi, R. Khasanov, M. Z. Hasan, H. Luetkens, and Z. Guguchia, Time-reversal symmetry-breaking charge order in a kagome superconductor, Nature (London) **602**, 245 (2022).

[24] H. Li, H. Zhao, B. R. Ortiz, T. Park, M. Ye, L. Balents, Z. Wang, S. D. Wilson, and I. Zeljkovic, Rotation symmetry breaking in the normal state of a kagome superconductor KV_3Sb_5, Nat. Phys. **18**, 265 (2022).

[25] Y. Xu, Z. Ni, Y. Liu, B. R. Ortiz, Q. Deng, S. D. Wilson, B. Yan, L. Balents, and L. Wu, Three-state nematicity and magneto-optical Kerr effect in the charge density waves in kagome superconductors, Nat. Phys. **18**, 1470 (2022).

[26] L. Nie, K. Sun, W. Ma, D. Song, L. Zheng, Z. Liang, P. Wu, F. Yu, J. Li, M. Shan, D. Zhao, S. Li, B. Kang, Z. Wu, Y. Zhou, K. Liu, Z. Xiang, J. Ying, Z. Wang, T. Wu *et al.*, Charge-density-wave-driven electronic nematicity in a kagome superconductor, Nature (London) **604**, 59 (2022).

[27] C. Guo, C. Putzke, S. Konyzheva, X. Huang, M. Gutierrez-Amigo, I. Errea, D. Chen, M. G. Vergniory, C. Felser, M. H. Fischer, T. Neupert, and P. J. W. Moll, Switchable chiral transport in charge-ordered kagome metal CsV_3Sb_5, Nature (London) **611**, 461 (2022).

[28] D. R. Saykin, C. Farhang, E. D. Kountz, D. Chen, B. R. Ortiz, C. Shekhar, C. Felser, S. D. Wilson, R. Thomale, J. Xia, and A. Kapitulnik, High Resolution Polar Kerr Effect Studies of CsV_3Sb_5: Tests for Time Reversal Symmetry Breaking Below the Charge Order Transition, Phys. Rev. Lett. **131**, 016901 (2023).

[29] W. Duan, Z. Nie, S. Luo, F. Yu, B. R. Ortiz, L. Yin, H. Su, F. Du, A. Wang, Y. Chen, X. Lu, J. Ying, S. D. Wilson, X. Chen, Y. Song, and H. Yuan, Nodeless superconductivity in the kagome metal CsV_3Sb_5, Sci. China: Phys., Mech. Astron. **64**, 107462 (2021).

[30] R. Gupta, D. Das, C. H. Mielke III, Z. Guguchia, T. Shiroka, C. Baines, M. Bartkowiak, H. Luetkens, R. Khasanov, Q. Yin, Z. Tu, C. Gong, and H. Lei, Microscopic evidence for anisotropic multigap superconductivity in the CsV_3Sb_5 kagome superconductor, npj Quantum Mater. **7**, 49 (2022).

[31] R. Gupta III, D. Das, C. Mielke, E. T. Ritz, F. Hotz, Q. Yin, Z. Tu, C. Gong, H. Lei, T. Birol, R. M. Fernandes, Z. Guguchia, H. Luetkens, and R. Khasanov, Two types of charge order with distinct interplay with superconductivity in the kagome material CsV_3Sb_5, Commun. Phys. **5**, 232 (2022).

[32] M. Roppongi, K. Ishihara, Y. Tanaka, K. Ogawa, K. Okada, S. Liu, K. Mukasa, Y. Mizukami, Y. Uwatoko, R. Grasset, M. Konczykowski, B. R. Ortiz, S. D. Wilson, K. Hashimoto, and T. Shibauchi, Bulk evidence of anisotropic *s*-wave pairing with no sign change in the kagome superconductor CsV_3Sb_5, Nat. Commun. **14**, 667 (2023).

[33] C. Mu, Q. Yin, Z. Tu, C. Gong, H. Lei, Z. Li, and J. Luo, S-Wave Superconductivity in kagome metal CsV_3Sb_5 revealed by $^{121/123}$Sb NQR and ^{51}V NMR measurements, Chin. Phys. Lett. **38**, 077402 (2021).

[34] H.-S. Xu, Y.-J. Yan, R. Yin, W. Xia, S. Fang, Z. Chen, Y. Li, W. Yang, Y. Guo, and D.-L. Feng, Multiband Superconductivity with Sign-Preserving Order Parameter in Kagome Superconductor CsV_3Sb_5, Phys. Rev. Lett. **127**, 187004 (2021).

[35] W. Zhang, X. Liu, L. Wang, C. W. Tsang, Z. Wang, S. T. Lam, W. Wang, J. Xie, X. Zhou, Y. Zhao, S. Wang, J. Tallon, K. T. Lai, and S. K. Goh, Nodeless superconductivity in kagome metal CsV_3Sb_5 with and without time reversal symmetry breaking, Nano Lett. **23**, 872 (2023).

[36] C. Zhao, L. Wang, W. Xia, Q. Yin, J. Ni, Y. Huang, C. Tu, Z. Tao, Z. Tu, C. Gong *et al.*, Nodal superconductivity and superconducting domes in the topological kagome metal CsV_3Sb_5, arXiv:2102.08356.

[37] Z. Guguchia III, C. Mielke, D. Das, R. Gupta, J.-X. Yin, H. Liu, Q. Yin, M. H. Christensen, Z. Tu, C. Gong, N. Shumiya, M. S. Hossain, T. Gamsakhurdashvili, M. Elender, P. Dai, A. Amato, Y. Shi, H. C. Lei, R. M. Fernandes, M. Z. Hasan *et al.*, Tunable unconventional kagome superconductivity in charge ordered RbV_3Sb_5 and KV_3Sb_5, Nat. Commun. **14**, 153 (2023).

[38] H. Tan, Y. Liu, Z. Wang, and B. Yan, Charge Density Waves and Electronic Properties of Superconducting Kagome Metals, Phys. Rev. Lett. **127**, 046401 (2021).

[39] J.-F. Zhang, K. Liu, and Z.-Y. Lu, First-principles study of the double-dome superconductivity in the kagome material CsV_3Sb_5 under pressure, Phys. Rev. B **104**, 195130 (2021).

[40] Y. Zhong, S. Li, H. Liu, Y. Dong, Y. Arai, H. Li, Y. Shi, Z. Wang, S. Shin, H. N. Lee, H. Miao, T. Kondo, and K. Okazaki, Testing electron-phonon coupling for the superconductivity in kagome metal CsV_3Sb_5, Nat. Commun. **14**, 1945 (2023).

[41] C. Wang, J. Yu, Z. Zhang, and J.-H. Cho, Phonon-mediated **S**-wave superconductivity in the kagome metal CsV_3Sb_5 under pressure, arXiv:2303.10080.

[42] X. Wu, T. Schwemmer, T. Müller, A. Consiglio, G. Sangiovanni, D. Di Sante, Y. Iqbal, W. Hanke, A. P. Schnyder, M. M. Denner, M. H. Fischer, T. Neupert, and R. Thomale, Nature of Unconventional Pairing in the Kagome Superconductors AV_3Sb_5 (A = K, Rb, Cs), Phys. Rev. Lett. **127**, 177001 (2021).

[43] M.-c. He, H. Zi, H.-x. Zhan, Y.-q. Zhao, C. Ren, X.-y. Hou, L. Shan, Q.-h. Wang, Q. Yin, Z. Tu, C. Gong, H. Lei, Z.-y. Lu, Q. Wang, Y.-p. Qi, G.-f. Chen, and P. Xiong, Strong-coupling superconductivity in the kagome metal CsV_3Sb_5 revealed by soft point-contact spectroscopy, Phys. Rev. B **106**, 104510 (2022).

[44] C. Wen, X. Zhu, Z. Xiao, N. Hao, R. Mondaini, H. Guo, and S. Feng, Superconducting pairing symmetry in the kagome-lattice Hubbard model, Phys. Rev. B **105**, 075118 (2022).

[45] X.-C. Bai, W.-F. Wu, H.-Y. Wang, Y.-M. Quan, X. Wang, Z. Zeng, and L.-J. Zou, Effective six-band model and unconventional spin-singlet pairing in kagome superconductor CsV_3Sb_5, New J. Phys. **24**, 123016 (2022).

[46] A. T. Rømer, S. Bhattacharyya, R. Valentí, M. H. Christensen, and B. M. Andersen, Superconductivity from repulsive interactions on the kagome lattice, Phys. Rev. B **106**, 174514 (2022).

[47] A. A. Tsirlin, P. Fertey, B. R. Ortiz, B. Klis, V. Merkl, M. Dressel, S. D. Wilson, and E. Uykur, Role of Sb in the superconducting kagome metal CsV_3Sb_5 revealed by its anisotropic compression, SciPost Phys. **12**, 049 (2022).

[48] Y. M. Oey, B. R. Ortiz, F. Kaboudvand, J. Frassineti, E. Garcia, R. Cong, S. Sanna, V. F. Mitrović, R. Seshadri, and S. D. Wilson, Fermi level tuning and double-dome superconductivity in the kagome metal $CsV_3Sb_{5-x}Sn_x$, Phys. Rev. Mater. **6**, L041801 (2022).

[49] T. Qian, M. H. Christensen, C. Hu, A. Saha, B. M. Andersen, R. M. Fernandes, T. Birol, and N. Ni, Revealing the competition between charge density wave and superconductivity in CsV_3Sb_5 through uniaxial strain, Phys. Rev. B **104**, 144506 (2021).

[50] F. Hardy, L. Wang, A. Shukla, A. A. Haghighirad, M. He, W. Xia, Y. Guo, and C. Meingast, Quantum oscillations in the kagome superconductors AV_3Sb_5 (A = K, Rb, Cs), 2023 APS March Meeting (2023), https://meetings.aps.org/Meeting/MAR23/Session/F27.3.

[51] See Supplemental Material at http://link.aps.org/supplemental/10.1103/PhysRevB.108.L100510 for details of the DFT calculations, details on the minimal tight binding model, details on the patch-model calculations, and a brief symmetry analysis, in addition to Refs. [52–58].

[52] G. Kresse and J. Hafner, *Ab initio* molecular dynamics for liquid metals, Phys. Rev. B **47**, 558 (1993).

[53] G. Kresse and J. Furthmüller, Efficient iterative schemes for *ab initio* total-energy calculations using a plane-wave basis set, Phys. Rev. B **54**, 11169 (1996).

[54] G. Kresse and J. Furthmüller, Efficiency of *ab initio* total energy calculations for metals and semiconductors using a plane-wave basis set, Comput. Mater. Sci. **6**, 15 (1996).

[55] W. Beugeling, J. C. Everts, and C. Morais Smith, Topological phase transitions driven by next-nearest-neighbor hopping in two-dimensional lattices, Phys. Rev. B **86**, 195129 (2012).

[56] H.-M. Guo and M. Franz, Topological insulator on the kagome lattice, Phys. Rev. B **80**, 113102 (2009).

[57] Y. Gu, Y. Zhang, X. Feng, K. Jiang, and J. Hu, Gapless excitations inside the fully gapped kagome superconductors AV_3Sb_5, Phys. Rev. B **105**, L100502 (2022).

[58] J. A. Sauls, A theory for the superconducting phases of UPt_3, J. Low Temp. Phys. **95**, 153 (1994).

[59] M. Y. Jeong, H.-J. Yang, H. S. Kim, Y. B. Kim, S. Lee, and M. J. Han, Crucial role of out-of-plane Sb *p* orbitals in van Hove singularity formation and electronic correlations in the superconducting kagome metal CsV_3Sb_5, Phys. Rev. B **105**, 235145 (2022).

[60] A. Consiglio, T. Schwemmer, X. Wu, W. Hanke, T. Neupert, R. Thomale, G. Sangiovanni, and D. Di Sante, Van Hove tuning of aV_3Sb_5 kagome metals under pressure and strain, Phys. Rev. B **105**, 165146 (2022).

[61] M. Kang, S. Fang, J.-K. Kim, B. R. Ortiz, S. H. Ryu, J. Kim, J. Yoo, G. Sangiovanni, D. Di Sante, B.-G. Park, C. Jozwiak, A. Bostwick, E. Rotenberg, E. Kaxiras, S. D. Wilson, J.-H. Park, and R. Comin, Twofold van Hove singularity and origin of charge order in topological kagome superconductor CsV_3Sb_5, Nat. Phys. **18**, 301 (2022).

[62] R. Nandkishore, L. S. Levitov, and A. V. Chubukov, Chiral superconductivity from repulsive interactions in doped graphene, Nat. Phys. **8**, 158 (2012).

[63] H. Isobe, N. F. Q. Yuan, and L. Fu, Unconventional Superconductivity and Density Waves in Twisted Bilayer Graphene, Phys. Rev. X **8**, 041041 (2018).

[64] L. Classen, A. V. Chubukov, C. Honerkamp, and M. M. Scherer, Competing orders at higher-order van Hove points, Phys. Rev. B **102**, 125141 (2020).

[65] D. V. Chichinadze, L. Classen, and A. V. Chubukov, Nematic superconductivity in twisted bilayer graphene, Phys. Rev. B **101**, 224513 (2020).

[66] D. V. Chichinadze, L. Classen, and A. V. Chubukov, Valley magnetism, nematicity, and density wave orders in twisted bilayer graphene, Phys. Rev. B **102**, 125120 (2020).

[67] Y.-M. Wu, R. Thomale, and S. Raghu, Sublattice interference promotes pair density wave order in kagome metals, arXiv:2211.01388.

[68] R. M. Fernandes, A. I. Coldea, H. Ding, I. R. Fisher, P. J. Hirschfeld, and G. Kotliar, Iron pnictides and chalcogenides: A new paradigm for superconductivity, Nature (London) **601**, 35 (2022).

[69] R. M. Fernandes, J. T. Haraldsen, P. Wölfle, and A. V. Balatsky, Two-band superconductivity in doped $SrTiO_3$ films and interfaces, Phys. Rev. B **87**, 014510 (2013).

[70] X. Chen, S. Maiti, A. Linscheid, and P. J. Hirschfeld, Electron pairing in the presence of incipient bands in iron-based superconductors, Phys. Rev. B **92**, 224514 (2015).

[71] S. Maiti, R. M. Fernandes, and A. V. Chubukov, Gap nodes induced by coexistence with antiferromagnetism in iron-based superconductors, Phys. Rev. B **85**, 144527 (2012).

[72] Y. Wang, J. Kang, and R. M. Fernandes, Topological and nematic superconductivity mediated by ferro-SU(4) fluctuations in twisted bilayer graphene, Phys. Rev. B **103**, 024506 (2021).

[73] Y. Zhong III, J. Liu, X. Wu, Z. Guguchia, J.-X. Yin, A. Mine, Y. Li, S. Najafzadeh, D. Das, C. Mielke, R. Khasanov, H. Luetkens, T. Suzuki, K. Liu, X. Han, T. Kondo, J. Hu, S. Shin, Z. Wang, X. Shi *et al.*, Nodeless electron pairing in CsV_3Sb_5-derived kagome superconductors, Nature (London) **617**, 488 (2023).